RESEARCH ARTICLE - APPLIED GEOPHYSICS

Rock physics-based analysis to discriminate lithology and pore fluid saturation of carbonate reservoirs: a case study

Esmael Makarian[1] · Ayub Elyasi[2] · Rasoul Hamidzadeh Moghadam[1] · Reza Khoramian[3] · Pedram Namazifard[1]

Abstract

Rock physics templates (RPT) and modeling contribute significantly to accurately and fast characterization of hydrocarbon reservoirs. This study strives to characterize lithology and pore fluid saturation for a carbonate reservoir in southwest Iran using RPT by well-logging data in a zone with a thickness of almost 100 m. To discriminate lithology, Greenberg–Castagna and Gardner models were applied. Also, velocity ratio—Gamma-ray (GR) and density—GR templates were implemented to investigate more. Results show that the researched zone's lithology consists of a considerable amount of limestone, followed by dolomite, and a small amount of shale, without sandstone, which matches excellently with the lithology column and geophysical logs. For fluid discrimination, two different rock physical directions were impalement. Firstly, the rock physics model of the study area was built through Xu and Payne's model. Then, velocity ratio—acoustic impedance template $(V_P/V_S–AI)$ was applied to modeled data scaled with resistivity and porosity and then successfully validated with oil and water saturation. Findings show that PRT organizes data concerning similar features (here, aspect ratio), causing easy, fast, and more accurate analysis, and fluid content in the study includes oil and water, which the figure for oil is much more. In different oil and water saturation, non-modeled data were investigated through $V_P/V_S − V_S$, $V_S − V_P$, and shear impudence (SI)—AI template supported by pore-pressure (PP) information to further research fluid distribution and its effect in the second direction. Regarding the rock physical analysis, the main reason for the decrease in seismic velocities and impedances is high pore pressure due to high oil saturation.

Keywords Rock physics · Greenberg and Castagna model · Gardner model · Lithology identification · Fluid discrimination · Carbonate reservoir

Introduction

Lithology

Reservoir characterization supplies geologists and petroleum engineers with valuable information on various rock and fluid properties playing an important role in managing and developing all stages of a hydrocarbon reservoir (Cross et al. 2022). Understanding lithology correctly can be advantageous to forecasting the volume of hydrocarbon in place and lessening uncertainty over reservoir characterization, for it is directly connected to porosity and permeability (Mondal and Singh 2022). There is a wide range of methods for lithology identification, one of which is utilizing coring samples and laboratory measurements such as microscopic image analysis (i.e., thin section) or other analyses like CT scans of cores and electron microscope (SEM) (Cao et al. 2022; Temizel et al. 2022). Extensive research has long been performed through well-logging data to distinguish lithology (Das and Chatterjee 2018; Islam et al. 2021), which recently using tools such as nuclear magnetic resonance (NMR) very much considered (Singh and Ojha 2022). Seismic analysis and seismic inversion are commonly used to determine lithology (Fawad et al. 2021; Radwan et al. 2022). Artificial intelligence (AI) methods have recently played a significant

✉ Ayub Elyasi
  a.elyasi1986@yahoo.com

[1] Department of Mining Engineering, Sahand University of Technology, Tabriz, Iran

[2] CAPE Consultant Group, Tehran, Iran

[3] Department of Petroleum Engineering, Nazarbayev University, Nur-Sultan, Kazakhstan

role in determining lithology (Taheri et al. 2022). A myriad of AI approaches was employed, which support vector machines (SVM), convolutional neural networks (CNNs), and deep learning (DL) methods are the most commonly used (Deng et al. 2017; Wang et al. 2022a, b; Xu et al. 2022). This point must be mentioned that in AI methods, information such as core, well–logging data, images, and seismic data are employed as data sets for input data. Electrofacies and geostatistics approaches are other techniques used to evaluate and identify lithology (Karimian Torghabeh et al. 2022; Mirhashemi et al. 2022). The mentioned methods are more likely to demand a great deal of money or be costly in some situations. In order to deal with the problems, rock physic techniques (RPT) can provide fast, easy, and accurate discrimination for underground projects. Many researches utilized PRT to discriminate lithology, some of which are listed as follows: (Huang et al. 2021; Hossain et al. 2022; Albakr et al. 2022).

Pore fluid saturation

Recognizing pore fluid distribution is a fundamental goal in oil and gas studies as it can control some vital parameters, such as pore pressure which is crucial in all stages of hydrocarbon investigations, especially for gas storage, enhanced oil recovery (EOR), and 4D seismic surveys (Elyasi et al. 2016; Pang et al. 2019). Various methods have been employed to pore fluid distribution in porous media. Laboratory test through coring samples is one of these, but it takes a lot of time and expenditure, and above all, maybe the fluid content of the samples will change due to the depth displacement and pressure changes (Wang et al. 2020). Well-logging information has another way (Das and Chatterjee 2018; Teillet et al. 2021). Numerous studies show that seismic-based methods were also used extensively to discriminate fluids. These methods use the impacts of fluids on seismic and elastic features, including velocities (Xu et al. 2021; Xie et al. 2022), amplitudes using amplitude versus offset (AVO), and impedances (Foster et al. 2021; Wang et al. 2022a, b), and frequency (Yang and Malcolm 2021; Lan et al. 2022). Other procedures also have been employed, such as geostatistics (Di et al. 2021; Grana et al. 2022), dual-porosity theory (Zhou et al. 2021; Li et al. 2022), elastic parameters and rock physics template (Ahmad et al. 2022; Abe et al. 2022), and intelligence methods (Chenin and Bedle 2022; Ibrahim et al. 2022).

Petroleum engineers and geologists desperately need to discriminate lithology and fluid content accurately and fast by employing available data and considering all conditions as much as possible in different conditions. Previous studies have used either very expensive and time-consuming methods or have high uncertainty. Furthermore, the preceding rock physics studies did not pay attention to using multiple

PRT to reduce uncertainty and increase accuracy in a short period and building rock physics modeling to organize and classify information for providing a quick look for discrimination. This study attempts to deal with the mentioned problems and improve the distinguishing lithology and fluid in hydrocarbon reservoirs. For this purpose, multiple rock physics templates and modeling were used simultaneously to evaluate their performance and cover all needed aspects. One of the great advantages of this study is that all results are validated through different information, tools, and scales; however, the preceding research used merely a few data to confirm. As a novel insight, this research uses rock physics modeling to engage geological features such as aspect ratio (AR) for pore fluid discrimination to transfer scattering data to organize with similar properties and validate with various parameters because one of the main goals of this study is to investigate rock physics patterns as much as possible. The research takes a further step and evaluates non-modeling data through PRT to discover events in the study area and compare them with modeling data.

Geological setting

The study area in southwestern Iran (Fig. 1) is in the Khuzestan province near the Abadan plain. A subsection of the Alpine–Himalayan belt, the area is considered part of the Mesopotamian Basin, next to the Dezful Embayment in the Zagros fold-and-thrust Belt (ZFTB). In general, the ZFTB has comprised several hydrocarbon reservoir formations, mainly carbonate, and different ages ranging from Triassic to Tertiary (Kordi 2019).

Two main elements have helped form these formations: different faults of this basin and distinct stages of Zagros folding dating back to early Cretaceous–late Tertiary. In particular, the surveyed region has been formed by the superimposition of late Tertiary folding due to Zagros Orogens. Being an Upper Cretaceous (Santonian) carbonate formation, the target region approximately has a maximum thickness of 100 m on average (AbdollahieFard et al. 2019). Stratigraphic studies of the carbonate formation show different fossils, namely Benthic, Rotalia, and Planktic foraminifera (Afghah 2016). Two shallow and deep facies exist in the carbonate formation, extending toward the northwest and southeast. However, this study is performed on the deep facies considered pelagic sediments (e.g., the inner neritic zone). The stratigraphic column of the study area can be seen in Fig. 2.

Regarding the geological structure, the study region is an anticline covered by alluvium sediments and is classified into shallow relief (Mehrabi et al. 2020). The anticline is an elongated structure with low-slope ridges and a west–northwest–east–southeast orientation. In this structure,
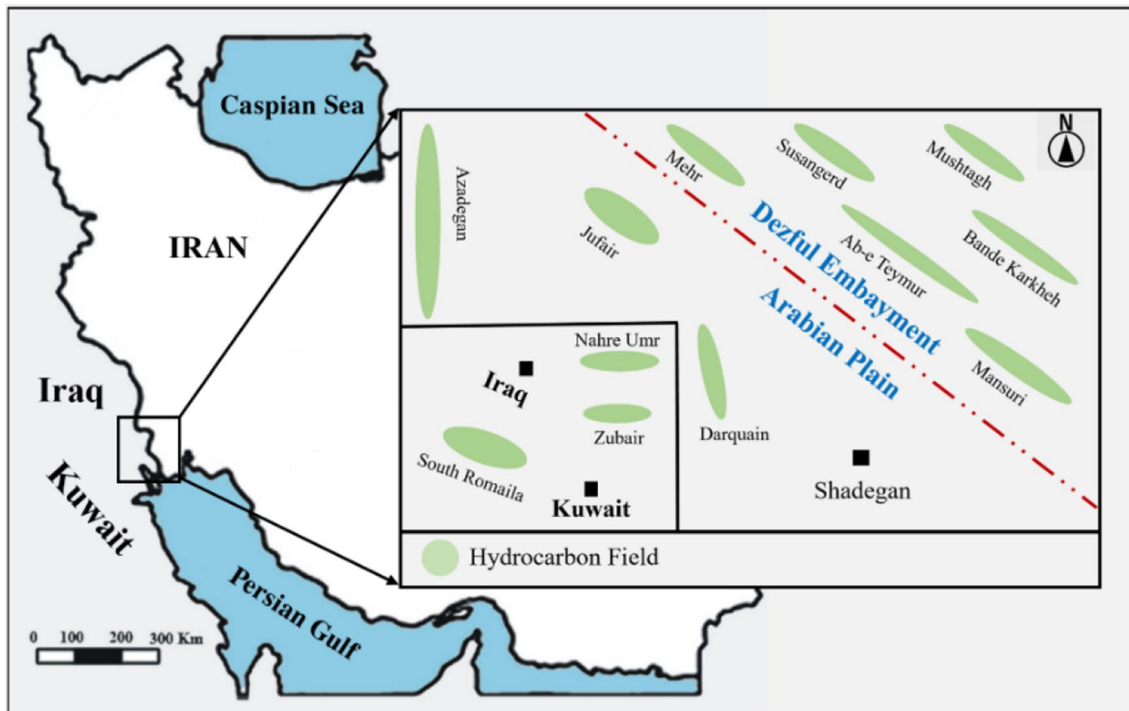
Fig. 1 Location map of the zone of interest

the northeastern ridges' slope is higher than the southeastern ones. From a lithological point of view, this carbonate formation comprises wackestone, packstone, gray packstone, porous, and partly dolomitic. Also, PVT experiments indicate that this formation is occupied with crude oil whose API gravity is almost 23. Other petrophysical properties, such as porosity, average water saturation, and shale percent, are reported to be 18.2, 20, and 8.5%, respectively.

Materials and methodology

This study aimed to diagnose the lithology and fluids type of a carbonate reservoir zone in the west part of Iran. A set of raw data obtained by well-logging operations was used. The raw data, being in LAS format, included these logs: density (RHOB), corrected gamma-ray (CGR), later log deep (LLD), porosity, P-wave velocity (V_P), S-wave velocity (V_S), water saturation (S_W), oil saturation (S_O), and volumes logs including the volume of shale, limestone(calcite), and dolomite. Due to the availability of each of the log data, none of them were empirically estimated. The preceding logs accessibility and their units are presented in Table 1. It should be noted that P-impedance and S-impedance were, respectively, calculated by multiplying P-wave velocity and S-wave velocity by density.

The workflow of this study was comprised of two main sections: (1) lithology and (2) saturation, which would be clarified further below.

Lithology

Quick-look identification

Intending to quickly know what kind of rock types there exists in the reservoir targets' zone, the log data of V_P, V_S, and RHOB were imported into RokDoc software, cross-plotted, and compared with two empirical rock physics models, Greenberg and Castagna (1992) and Gardner et al. (1974). The former combines P-wave and S-wave velocities, and the latter connects RHOB to P-wave velocity for lithological discrimination. These two models developed through the laboratory evaluations of distinct rock types greatly assist petrophysicists. The reason for using the empirical models was that both seismic data (body waves) and the intrinsic rock data of density had been individually involved in the models, reflecting any lithology changes.

Rock physics templates

Rock physics models and templates were introduced by Ødegaard and Avseth (2004) as a magical methodology for forecasting lithology and fluids. These charts, known as cross-plots, have been used frequently to connect seismic variables with non-seismic to visually detect any irregularities in the reservoirs (Gelinsky 2020). Herein, two cross-plots were selected and plotted, including V_P/V_S versus

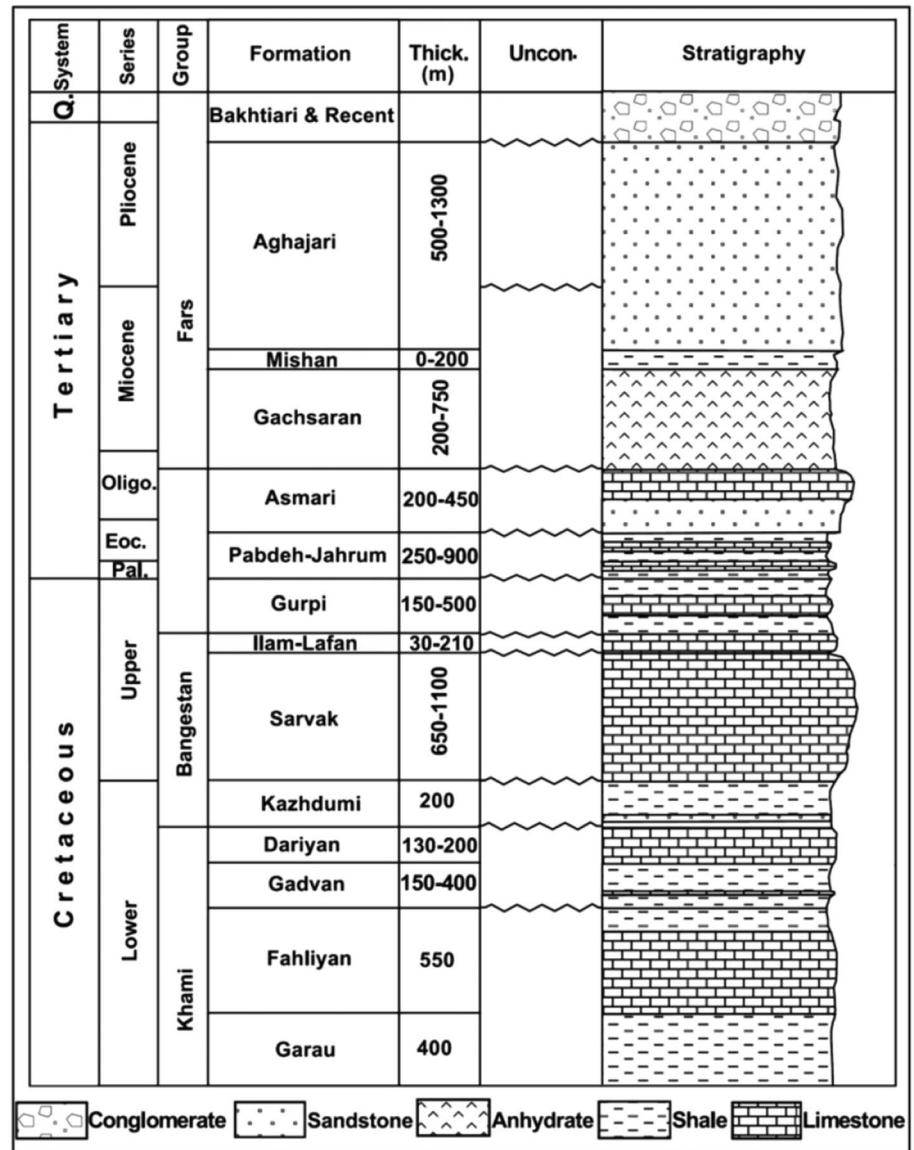**Fig. 2** Sequence stratigraphy of the study area (Alavi 2004)

Table 1 The well-logging data used in this survey with their standard units are available

RHOB (g/cm³)	CGR (API)	LLD (Ω-m)	Porosity (fraction)	V_P (m/s)	V_S (m/s)	S_W (fraction)	S_O (fraction)	Volume logs (fraction): shale—limestone—dolomite
✓	✓	✓	✓	✓	✓	✓	✓	✓

CGR and RHOB versus CGR. Then, an in-depth analysis was made on them to find a direct relationship between the intrinsic rock data (of RHOB and CGR) and the seismic parameters (of V_P and V_S) for lithological distinguishment because multifarious clustering options have been introduced to differentiate shale from limestone, sandstone, and dolomite using the cross-plots (Avseth and Mukerji 2002).

Well-logging analysis

The gamma-ray logs, formation density, and neutron porosity were then used and interpreted to validate the lithology differentiations. Being highly impacted by rock characteristics and slightly impacted by fluid characteristics, the logs are the finest for lithological delineations (Zhou et al. 2018).

Saturation distinguishment

Saturation is one of the most critical data for many reservoir engineering calculations (Yang and Wei 2017). P-wave velocity (V_P) is useful, practical petrophysical data for pore fluids detection. There exists adequate evidence that V_S (S-wave velocity) is highly likely to help identify the fluid type (Avseth et al. 2010). Combining S-wave and P-wave velocities might help engineers with fluid-type discrimination (Pang et al. 2019). Acoustic impedance (AI), also called P-impedance, is an effective technique for distinguishing among pore fluids. The cross-plotting approach has drawn too much attention to calculating fluid saturation (Mavko et al. 2020). Herein, AI–V_P/V_S cross-plot, introduced by Ødegaard and Avseth (2004), was opted for and used as a fluid diagnostic tool. In addition to the two parameters of velocity ratio (V_P/V_S) and P-impedance (AI), resistivity log (LLD) variations were also investigated for the zone of interest to infer information about the presence of water or hydrocarbons. To better organize the velocity ratio data, V_P and V_S velocities were modified using the multiporosity model of Xu and Payne (2009). Building Xu and Payne (2009) in this case study involves several steps as follows (Fig. 3):

(a) Mixing different lithologies by Reuss–Voigt–Hill (RVH) average equations to build a solid rock matrix (SRM).
(b) Adding pore type to SRM through pore aspect ratio (AR) from sedimentology analysis utilizing differential effective medium (DEM) theory and Kuster and Toksöz's (1974) model to make dry rock module (DRM).
(c) Mixing fluids using Wood equation (1955).
(d) Adding the mixed fluid to DRM using the Gassmann equation (1951) to build fluid-saturated rock (FSR).

The mixing law of the Reuss–Voigt–Hill was initially used for mixing the minerals present in the solid matrix because each component has a different elastic characteristic that must be taken into account when mixing, so that

the rock physics model can be built within the boundaries according to its performance characteristics (Avseth et al. 2010). Clay pores (e.g., micron-sized pores filled with bound water) were next inserted into the solid matrix by applying the effective differential medium (DEM) model (Xu and Payne 2009). To consider the pores' diameter when estimating V_P, V_S, and density, the theory of Kuster and Toksöz (1974) was also employed. To do so, the parameter of pore aspect ratio, whose values were provided from the sedimentological information of the study zone (see Table 2), was applied based on the previous theory.

Using the DEM model, two other micron-sized pores, e.g., water-wet and dry (non-bond-water), were inserted into the solid matrix system, aiming to calculate the bulk modulus of the dry solid matrix.

The residual water with the hydrocarbons of oil and gas was mixed using the suspension model of Wood (1955), and then, the V_P value for the fluids was estimated (Avseth et al. 2010). After that, the fluids' system was added to the dry rock system using the Gassmann equation. The objective was to measure the bulk modulus for the fluid-saturated rock system and observe how the fluid addition would influence the seismic properties. Considering pores' average diameter was found to help particles with similar properties set together (Li and Zhang 2018). The intrinsic rock property of porosity has established a close relationship to the presence or absence of fluids in the reservoir rocks—a high porosity in a reservoir is bound to the company of a considerable amount of fluids (Qing et al. 2020). Thus, the porosity effect on fluids distribution within the zone of interest was separately examined in another AI–V_P/V_S cross-plot scaled with the porosity values. The cross-plot was also scaled with oil saturation (S_O) and water saturation (S_W) and analyzed to

Table 2 The aspect ratio for different lithologies in the studied zone

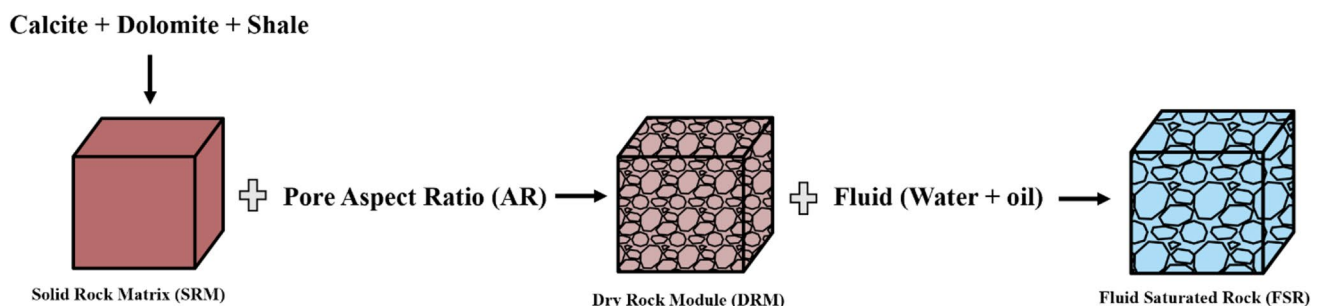| Lithology	Limestone (calcite)	Dolomite	Shale
Aspect ratio (AR)	0.18	0.17	0.08

Fig. 3 Workflow for building rock physics model (Xu and Payne 2009) in the study area

correlate the involved parameters to each other, attempting to recommend a local rock physics template. A new series of cross-plots were designed and closely investigated to verify the results obtained from the cross-plots. Avseth et al. (2010) suggested two cross-plots: V_P/V_S versus V_S and V_P versus V_S. The higher sensitivity of P-wave velocity to fluid changes than S-wave velocity was the reason for choosing the cross-plots. The popular cross-plot of S-impedance (SI) versus P-impedance (AI) was also used to regard the non-seismic parameter of density in pore fluid prediction (Avseth et al. 2010). It should be emphasized that the verification was performed using the well-logging data, not the modeling one, and also by applying S_O and S_W simultaneously.

Results and discussion

Lithology discrimination results

Quick-look evaluation results

The compressional and shear wave velocities data were plotted versus each other and fitted with Greenberg and Castagna's empirical model (1992) to guess the possible lithology in the study zone quickly. The results are shown in Fig. 4, in which X-axis represents V_S and Y-axis represents V_P.

The sandstone line crossed no point on the cross-plot and fell at the bottom of the data points, expressing that no sand existed in the zone. Many scatter points perfectly matched the two lines of limestone and dolomite, showing significant lithologies. Only a tiny amount of the data points was fitted with the shale line, indicating a low-shale formation. Therefore, three particular lithology types could be identified based on the cross-plot of Greenberg and Castagna (1992) and the seismic velocities of V_P and V_S. Nonetheless, limestone was quite recognizable as the dominant lithology. The lithology prediction could be justified based on the CGR scale (Fig. 4), a reliable indicator of rock mineralogy (Dong et al. 2016). The yellow, orange, and red points were identified as shale lithology due to being overlaid with Greenberg and Castagna's shale line. The points being of CGR values above 20 API designate the presence of marl, shale, or minerals with high levels of potassium (K[19]) and thorium (Th[90]) because shaley formations commonly release more elevated amounts of gamma-ray than the rest of sedimentary rocks (Asquith et al. 2004). The dark, bright, and pale blue points, which were found to be of limestone and dolomite mineralogy, possess CGRs below 20 API. Generally, CGRs lower than 20 API are attributed to sandstone, limestone, and dolomite (Nazeer et al. 2016). However, because Greenberg and Castagna's sand line did not cross any of the points, the CGRs herein merely corresponded to limestone and dolomite.

In the previous section, lithology discrimination was made only based on the amounts of seismic velocities. The experimental model of Gardner et al. (1974) was also utilized to ensure the already-made discrimination. Unlike
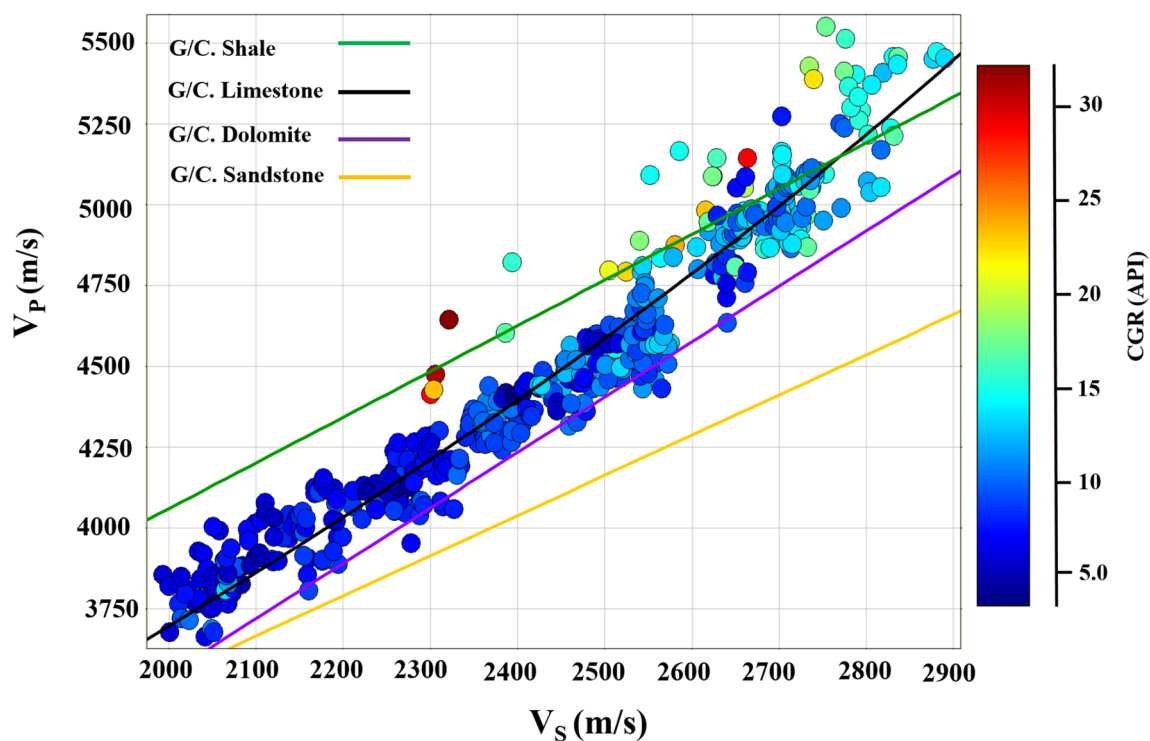

Fig. 4 The cross-plot of V_P versus V_S fitted with Greenberg and Castagna's model (1992)

Greenberg and Castagna's model (1992), the parameter of formation density (RHOB), which is affected by both rock and fluid properties, is applied in this model for marking out the lithologies. The cross-plot of RHOB versus V_P is presented in Fig. 5.

The lithology results of this chart were in good agreement with those of Greenberg and Castagna. Similarly, a few data points were overlaid with Gardner's shale line, restating that a small amount existed. The best line fitted on the data was limestone, followed by dolomite as the second-best. Observing such behavior dictated that the reservoir zone of interest mainly comprised dolomite and limestone. The shaley points were of higher RHOB and placed in the range of more P-wave velocity, whereas the trend was the opposite for dolomite and limestone points, possessing lower V_P and RHOB. It was probably because of the higher porosity of this area, meaning that they could accommodate more fluid than the shaley area (Crain 2013).

Rock physics templates findings

The shear and compressional transient time values can be utilized for quick-look lithology discrimination based on the P-wave to S-wave velocity ratio (V_P/V_S) (Avseth and Mukerji 2002). The ratio of V_P/V_S was hence plotted versus CGR values (Fig. 5) to differentiate the target zone in terms of lithology. Crain's thumb rules say that V_P/V_S for shale is higher

than 1.90, and the figure for limestone is between 1.80 and 1.95. Dolomite will also be of V_P/V_S 1.65 to 180. It, for sandstone, will range from 1.55 to 1.65. Using the V_P/V_S and CGR values recommended in Crain's petrophysical handbook (Crain 2013) for different lithologies, the reservoir area was subdivided into three zones, shale, dolomite, and limestone as follows. Looking at Fig. 6, CGR values higher than 20 API and V_P/V_S more than 1.90 show a few shaley points highlighted by a black oval. This implies that the target zone contains a small amount of shale. CGRs below 20 API may also indicate limestone, dolomite, or sandstone since there is no exact amount of CGR in the literature to discriminate these three lithologies.

We looked at the values of V_P/V_S as a good lithological indicator based on Crain's rules of thumb. Almost two-thirds of the points had V_P/V_S 1.80–1.90, and about one-third had V_P/V_S 1.65–1.80, which were inferred to be limestone (red oval) and dolomite (yellow oval), respectively. However, there were no points V_P/V_S less than 1.65, indicating sandstone. These results, being in good agreement with Greenberg and Castagna's or Gardner's cross-plots, reassure that limestone is the primary lithology of the target zone, whereas sandstone had no contribution whatsoever.

The cross-plot of density (RHOB) with the corrected gamma-ray (CGR) was also generated to more accurately delineate the various lithologies of the area of interest. Choosing this specific cross-plot was to involve RHOB for
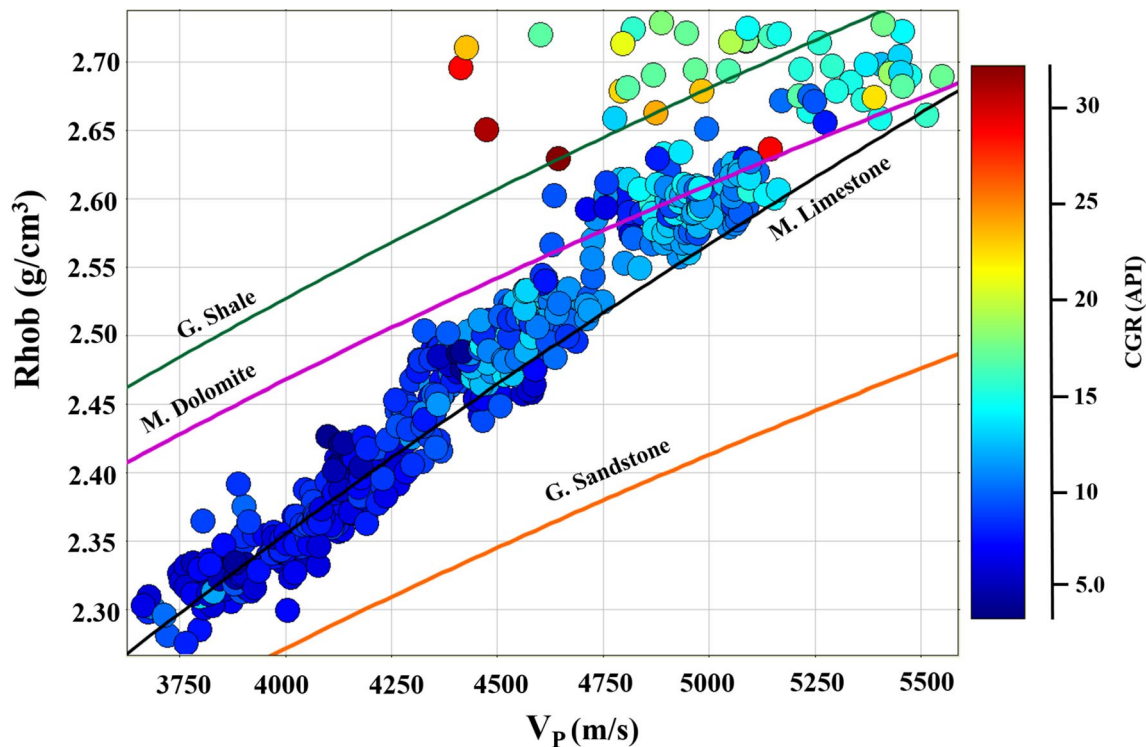

Fig. 5 The cross-plot of RHOB versus V_P for the study area is based on Gardner's model
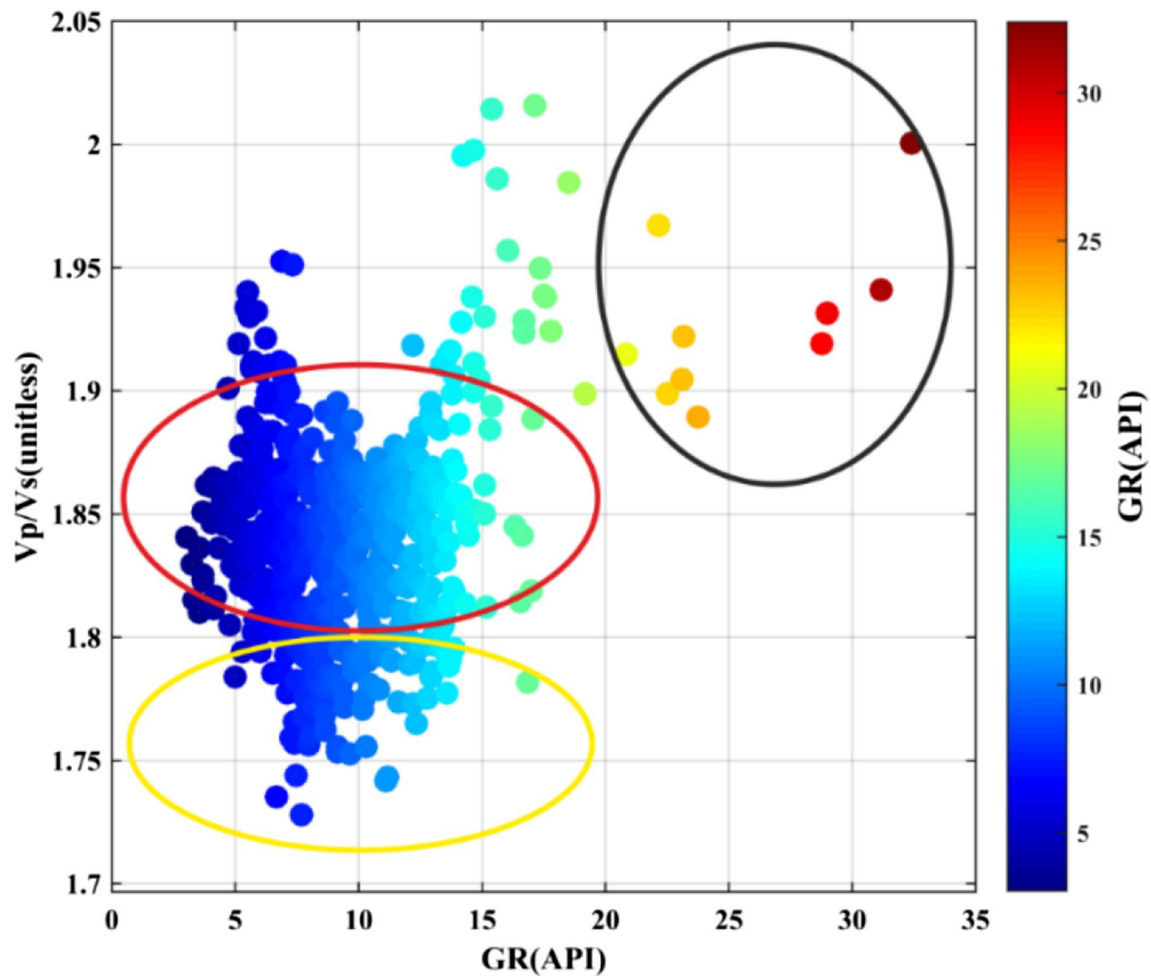
Fig. 6 The cross-plot of V_P/V_S against CGR for the study area

better lithology identification. Plotting RHOB versus CGR in well AB indicated four clusters (Fig. 7). The first cluster, highlighted with a black oval, contains the points with CGRs higher than 20 API and densities higher than almost 2.63 g/cm³. This cluster was named shale because shales have high gamma ray and high rigidity—the more the rock rigidity, the higher its density. The lithology for the region where CGR is lower than 15 API cannot be shale, thanks to the low amount of gamma-ray. Plus, since it has already been found that the study region is not made of any sand, this area (CGR < 15 API) should be merely composed of dolomite and limestone. The lithology for where density ranged from 2.55 to 2.7 g/cm³ was guessed to be dolomite (yellow oval) because the bulk density of dolomite is more than that of limestone.

And for where density was below 2.55 g/cm³, the lithology was selected to be limestone (red oval). Different fluids in the target zone might justify the tangible difference in the density values. The part with lower densities might be occupied with hydrocarbon, and the position with higher densities could be filled with water. The green points had

CGRs 15–20 and were determined to be intercalation of shale and limestone (blue oval). When two different depositional environments are in close spatial proximity, they are likely to migrate preferably across the contact and streak through each other. It is to be pointed out that all lithologies change completely gradually in the study area, and there are no certain borders among them. This is due to the similar properties of calcite and dolomite (Wei et al. 2020), which make up a large percentage of the lithologies.

Well-logging assessments

So far, well logs have been utilized to have a concise, precise view of formation characteristics at different depths of reservoirs. This study used the CGR, RHOB, and neutron well logs to justify the lithology identification. Looking at Fig. 8, which depicts the findings of the four preceding well logs, it can be viewed that the CGR values recorded versus depth laid in the range of nearly 3–34 API, being very low. The small area possessing CGR amounts of more than 20
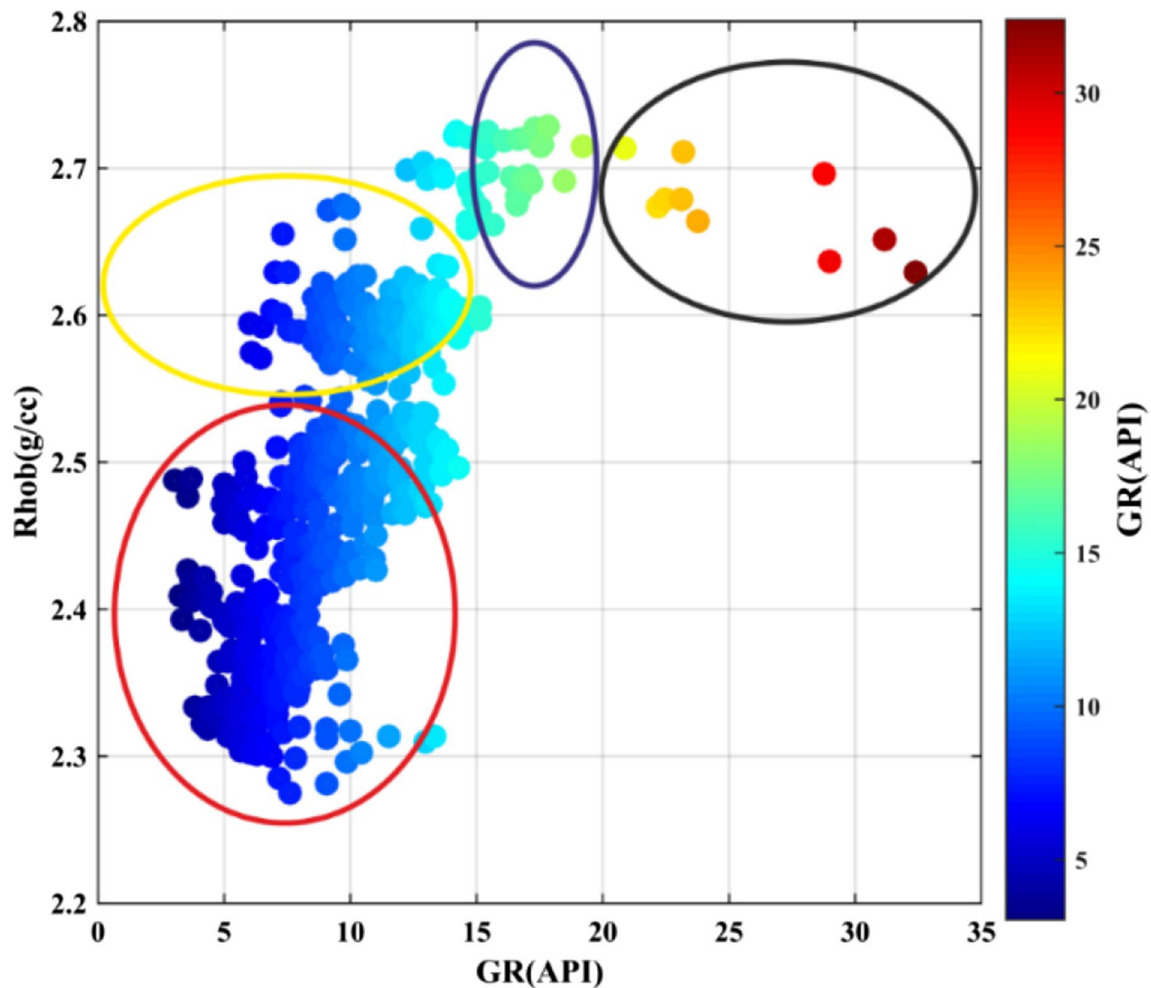
Fig. 7 The cross-plot of RHOB against CGR for the study area

API (2933–2940 m) confirmed the existence of a negligible quantity of shale in the survey zone. Although the shaley area constituted a minor part of the survey zone, a significant part of the zone, CGRs less than 20 API, accounted for a carbonate formation, either limestone, dolomite, or a combination of both (2940–3020 m). Such findings were verified by the position of the density and neutron logs, which is the most well-founded indicator of distinct lithologies. Limestone was the study zone's primary lithology since the density log had generally laid to the right of the neutron. However, the trend was reversed in the first few meters of the zone, showing the presence of shale. As far as saturation is concerned, the less density, the further the oil saturation. At first, where density was so high (shaley zone), it was deduced that the shaley zone was filled with water. But then, where density decreased gradually, and neutron fell considerably, oil saturation experienced significant growth, reaching its maximum at a depth of 2963 m. The logs of density and neutron met each other. Beyond the depth, the former saw a progressive decrease, and the latter suffered from a

significant increase, implying that oil saturation declined and water saturation inclined. In conclusion, limestone was the primary lithology, whereas there was a minor shale in the first part of the studied depth.

Saturation results and sensitivity study of rock physics modeling data

As explained in the methodology section, Xu–Payne's model (2009) was utilized to determine saturation in the interest zone. Involving geological factors, the rock physics model helps provide a more accurate estimate of the unknown data. The VP, VS, RHOB, and AI parameters were modeled using the preceding rock physics model in this connection. Before using the parameters, their compatibility with the real data points was investigated via the R-squared (R^2) coefficient to assure reliability. R^2 is a statistical goodness-of-fit index showing how well the modeled data match the real data in linear regression. R^2 values, which generally lie between zero and one, are commonly reported percentages from zero
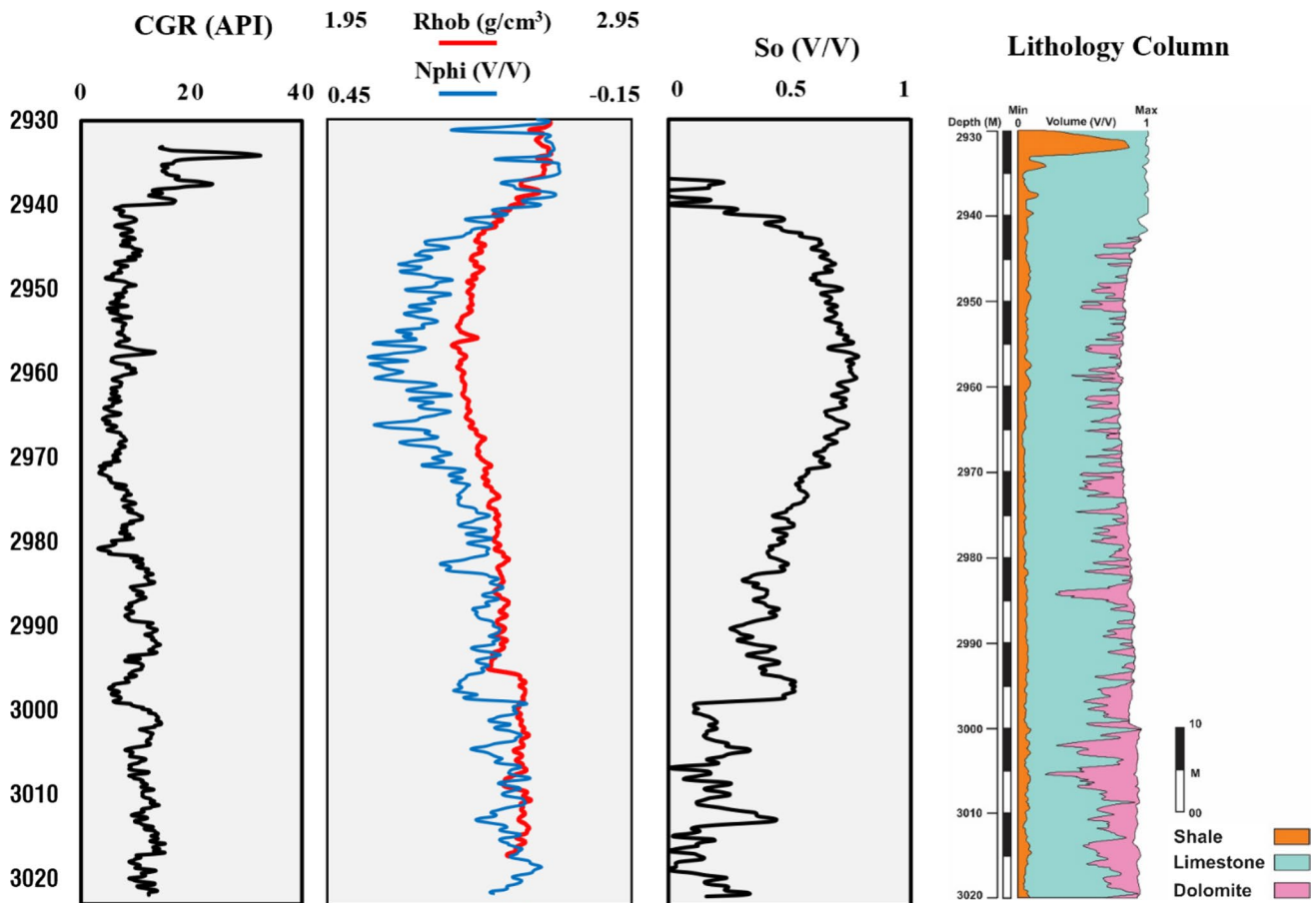
Fig. 8 Well-logging data and lithology column for the study area

to one hundred. In general, the higher R^2, the better match for the model. As shown in Fig. 9, different values of R^2 were obtained for the four parameters of V_P, V_S, RHOB, and AI.

The proportions of R^2 for RHOB and AI were the highest and quite similar, at almost 97% and 93%, respectively (Fig. 9c–d). This means there is only a slight difference of three-to-seven percent between the matched values and the observed data regarding density and acoustic impedance. Also, while R^2 accounted for 88% of V_P, this figure was slightly lower for V_S, at 78% (Fig. 9a, b). In other words, there are higher differences between the modeling data and the raw data for this data set. The density estimation is so good because the total density (the density of the rock and fluid) has remained unchanged. The lithology column in Fig. 6 is predominantly carbonate, and the fluids are mostly oil. So lithological changes, including rock and fluid changes, should not have changed much. As for S-wave and P-wave velocities, the estimation of compressional wave velocity has been better than the shear one. This is because V_P is more sensitive than V_S to porous media contents like fluids (Assefa et al. 2003). Thus, impedance (AI) estimation,

which is the product of the compression wave velocity by density, is acceptable.

Modeling data

Due to the high sensitivity of P-wave velocity (V_P) and P-impedance (AI) to fluid changes (Pang et al. 2019), the cross-plot of AI–V_P/V_S color-coded with a deep resistivity log (LLD) was employed to characterize the zone of interest in terms of fluid content. To solve the problem of data scattering, the V_P/V_S was modified using the DEM model and used as V_P/V_S.DEM. As can be seen in Fig. 10a, there is a linear relationship between the modified velocity ratio and the acoustic impedance.

Low AI and V_P/V_S values are associated with high resistivity values and vice versa. To justify this trend, two possible theories are suggested, one of which will be rejected: it is due to (1) the existence of any fluid in the pore system and (2) the co-existence of two or more fluids. As for theory one, it is thought that a high-density rock without any fluid should be responsible for high resistivity. A rock system simultaneously has a higher resistivity, AI, and V_P/V_S than fluids. In
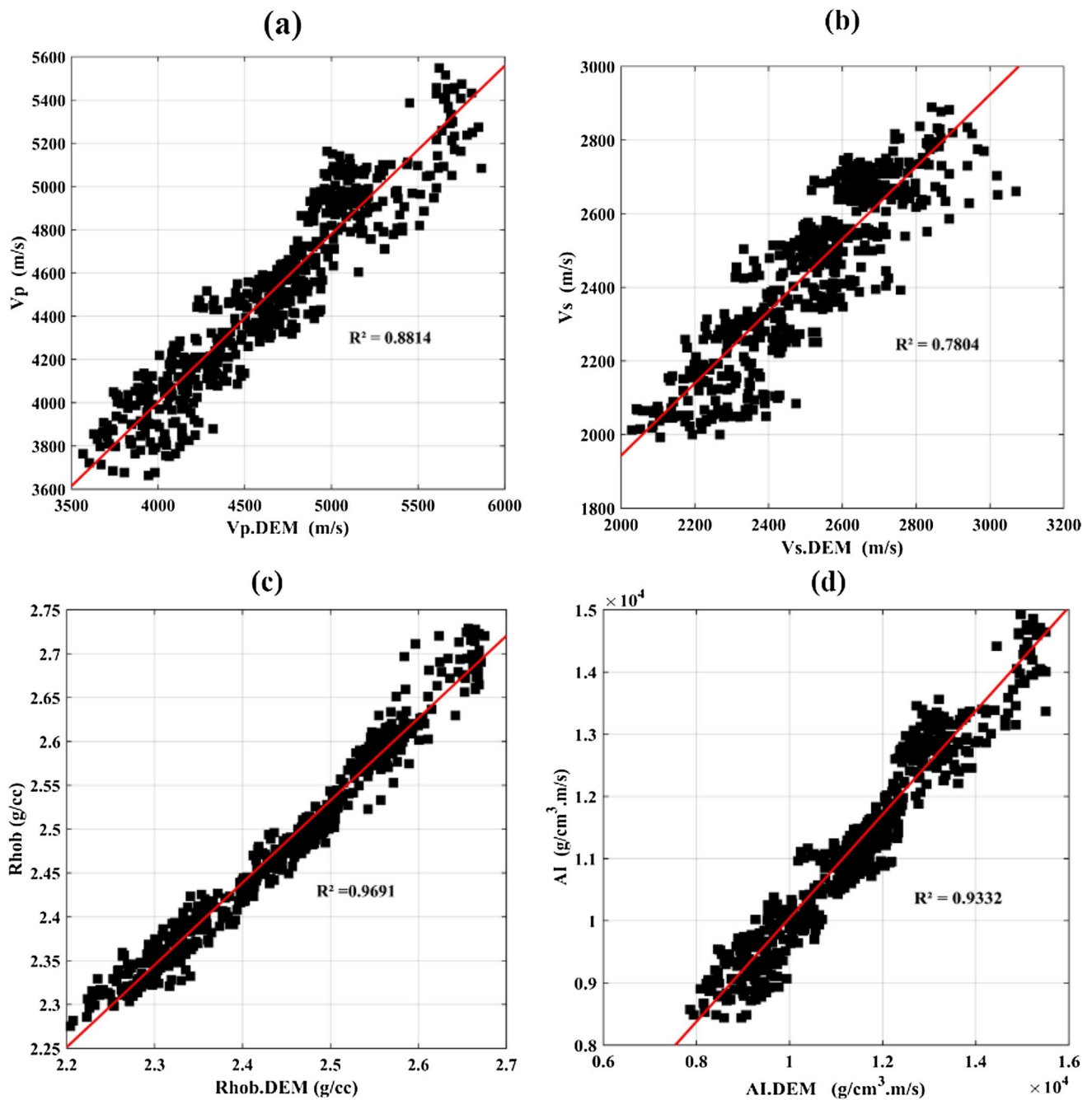
Fig. 9 Correlations between **a** V_P versus V_P. DEM with $R^2 = 0.88$, **b** V_S versus V_S. DEM with $R^2 = 0.78$, **c** RHOB versus RHOB.DEM with $R^2 = 0.96$, and **d** AI versus AI. DEM with $R^2 = 0.93$

Fig. 10a, where the resistivity is high, the other two (AI and V_P/V_S) are not high but low, meaning that theory No. 1 is incorrect. The pore system is occupied with different fluids of different densities (theory No. 2). Considering resistivity values, it can be deduced that when resistivity is high, and AI and V_P/V_S are low, a low-density, low-conductivity fluid like oil is filled into the pore system. Also, when AI and V_P/V_S are high and resistivity is low, a high-density, high-conductivity liquid like water should exist in the porous media. And a mix of water and oil occupies the pore system when resistivity, AI, and V_P/V_S are mean. This is because all the parameters are highly correlated; the more density, the more AI and V_P/V_S, and the less resistivity. In the following, the color bar of resistivity is substituted with that for porosity to verify theory No. 2 is accurate (Fig. 10b), where resistivity shows a high value in Fig. 10a and porosity has a
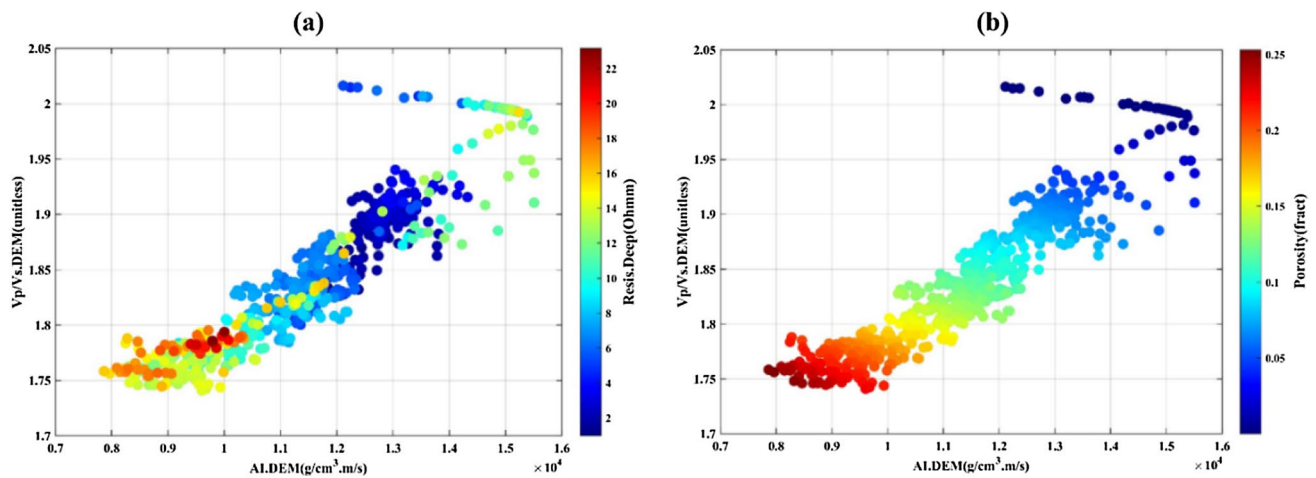
Fig. 10 The cross-plots of V_P/V_S. DEM versus AI. DEM scaled by **a** deep resistivity and **b** porosity

high value in Fig. 10b, proving the presence of a tremendous amount of fluid.

On the contrary, high values of V_P/V_S and AI represent low porosity and resistivity, which is to say the rock is so dense that it might have no pores or its pore space is low. This area is more likely to be occupied with high density and conductivity fluid. It is now evident what type of fluids is filled into the zone of interest. When a porous medium's porosity increases, its fluids' volume increases. Consequently, the density and the seismic velocities decrease (Borgomano et al. 2019). The propagation of seismic waves in a porous medium depends very much on the elastic properties of the porous medium and its density. Therefore, the denser the rock, the higher the seismic velocities and acoustic impedance, and vice versa (Boxberg et al. 2015). AI–V_P/V_S was also plotted with

known oil saturation (S_O) and water saturation (S_W) color bars (see Fig. 11) to prove the accuracy of what has been anticipated so far.

As expected, high oil saturation (Fig. 11b) or low water saturation (Fig. 11a) is seen at low values of AI and V_P/V_S exactly where resistivity (Fig. 10a) and porosity (Fig. 10b) are high, which conveys good coordination with the previous results. To conclude, when porosity and resistivity are high, or AI (density) and V_P/V_S are low, it is expected to have the most oil and the least water. V_P and V_S decrease in a region filled with oil because oil has a lower density than water and is sensitive to density. As a result of seismic velocities and density reduction, acoustic impedance also decreases. The concept of acoustic impedance is the acoustic resistance of a porous medium against the propagation of waves so that with an increase in density, this resistance increases and vice versa. Hence, acoustic impedance decreases due to
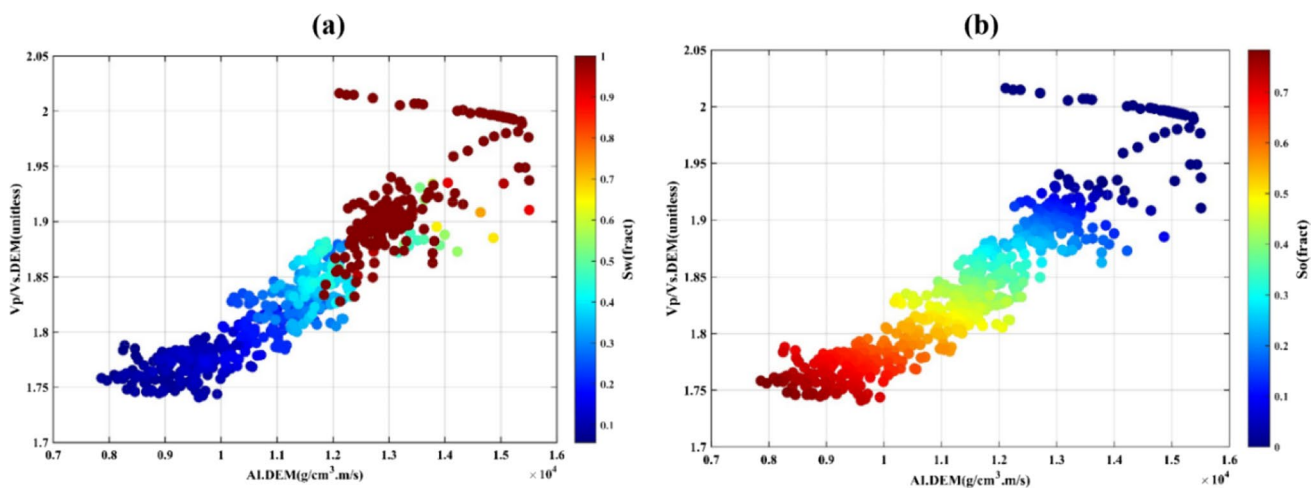

Fig. 11 The cross-plots of V_P/V_S. DEM versus AI. DEM scaled by **a** water saturation and **b** oil saturation

the lower oil density than in water, where more oil is seen (Li and Peng 2017).

Non-modeling data

The previous section measured fluid distribution using modeling data, fluids resistivity, and rock porosity. It was proven that the less AI and V_P/V_S, the more porosity and fluids of high resistivities, like oil. This section aims to estimate fluid saturation using non-modeling (well-logging) data and the parameter of fluid density. It is related to both V_P and V_S. Considering this in mind, the velocity ratio of V_P/V_S was plotted versus V_S at different saturations of oil and water (Fig. 12) to find a relationship among them.

In this plot, $S_O \geq 0.7$ (oil zone) delineated by the little triangular black dots demonstrates low values of V_S, and $S_W \geq 0.8$ (water zone) specified by the dark blue circular dots represents high values of V_S. Stated alternatively, water saturation (S_w) experiences a gradual upward trend when P-wave velocity increases and oil saturation (S_O) decreases steadily when P-wave velocity proceeds to increase. S-wave velocity (V_S) is directly and inversely proportional to the square root of shear modulus (μ) and density (ρ). Also, oil density is much lower than water, and the shear modulus is constant. It is thus expected to see a lower V_S for the oil zone than the water zone; however, this trend is entirely reversed in Fig. 12. This behavior may be related to the high volume of oil in the study area affecting seismic velocities. Lee (2003) reported that when oil saturation increased in a

hydrocarbon region with relatively high and abnormal pressures, V_S would reach its minimum value, whereas it should be maximum. Our results, which agree with previous studies, are shown in Fig. 13, color-coded with oil saturation. The highest oil saturation was seen when V_S was minimum and vice versa.

The cross-plot of S-wave velocity (V_S) against P-wave velocity (V_P) was alternatively used for further confirmation. A linear behavior governs V_S and V_P, as shown in Fig. 14.

Again in this figure, higher oil saturation is achieved at lower values of the velocities. In contrast, as previously explained, water saturation is achieved at higher velocities values due to the high oil pore pressure. This graph signifies that where a more compressible, lighter fluid-like oil saturates porous media, it should be expected to have lower V_P and V_S and conversely for water, which is an almost incompressible and heavier fluid. The cross-plot of S-impedance (SI) versus P-impedance (PI) was finally investigated to consider the simultaneous impact of the velocities and density on pore fluids distribution. As presented in Fig. 14, the oil-saturated zone ($S_O \geq 0.7$) can be differentiated by a reduction in both acoustic impedances compared to the water-saturated zone ($S_W \geq 0.8$). Oil presence decreases AI and SI, and water presence increases AI and SI (Fig. 15). The oil's lower density and bulk modulus cause a decrease in the total density and V_P, leading to a considerable reduction in AI and SI. In agreement with other studies (Fawad et al. 2020), the results express that different P-wave and S-wave velocities inside a reservoir would reflect different fluid saturations.
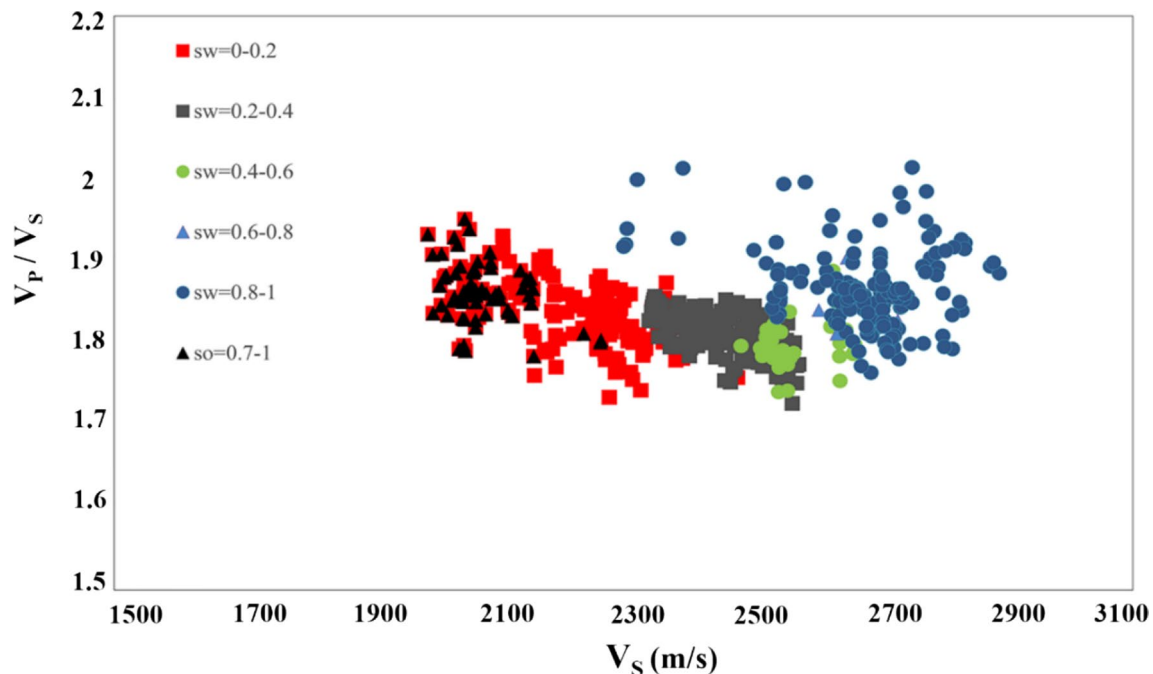

Fig. 12 The cross-plot of V_P/V_S against V_S was scaled by different oil and water saturation values
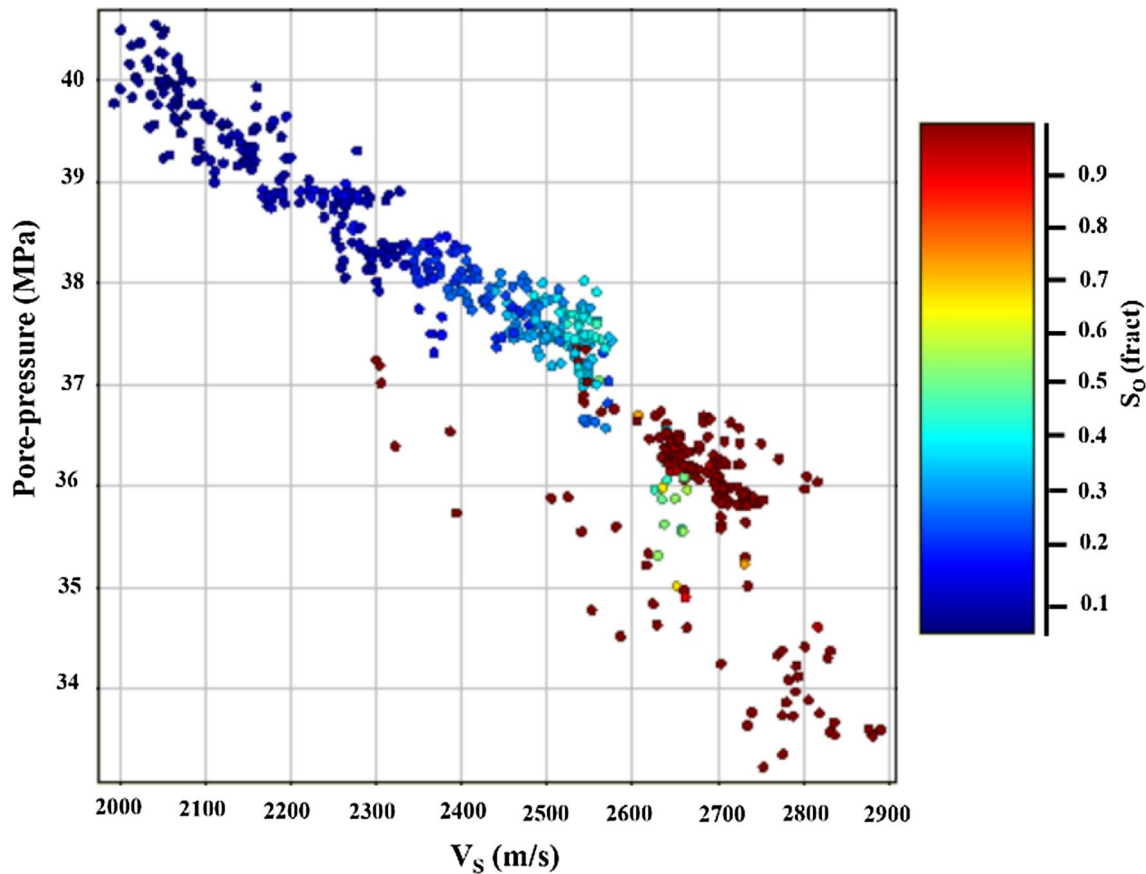
Fig. 13 The cross-plot of pore-pressure versus V_S scaled by oil saturation

Conclusions

The present investigation indicated that rock physics templates could yield a proper qualitative characterization of lithology in the area under study. Greenberg and Castagna's (1992) and Gardner et al. (1974) empirical rock physics models helped identify lithologies quickly. It also confirmed that the cross-plots of V_P/V_S-CGR and RHOB-CGR could be used as an alternative tool to rapidly and effectively differentiate lithologies, since lithology classifications using those yielded broadly similar results to those derived from well logs. Limestone and dolomite constituted the primary lithology, and shale the minor lithology. On the contrary, the target zone was composed of no sand. The shale area had higher V_P and RHOB than dolomite and limestone, perhaps due to less or no fluid. Regarding fluid distribution, it was discovered that as P-impedance (AI) and the velocity ratio (V_P/V_S) descended, porosity and fluid saturation with low conductivity (high resistivity) ascended. In other words, the pay zone was maximally occupied with oil when porosity and resistivity were maximum, or V_P/V_S and AI were minimum. These two seismic factors (V_P/V_S and AI) were thus found to be so powerful for reservoir fluids discrimination

using the cross-plot analysis. This method could be applied more effectively when the theory of DEM corrected the velocity ratio of V_P/V_S. This theory provided conditions where most data points were positioned more regularly and a linear relationship governed by the cross-plot of AI and V_P/V_S. DEM. It was also understood that when oil pore pressure was relatively high, V_S values would be minimum because a lower V_S was seen in the zone of interest where oil volume was high, causing an abnormal pressure.

The methods and techniques used in this research have some limitations that can be improved in the next studies. This research was carried out in an area with moderate porosity; the utilized RPT and models do not work in areas with high porosity, tight sands, shaly and laminated sands, so it is suggested to conduct rock physics analysis in an area with the mentioned characteristics and try to build a local rock physics model for it that can help in the discrimination of fluids and lithology. Additionally, here, we successfully applied some RPT in new directions and insights to discriminate pore fluids and lithology with enough data, but in some areas, maybe there would not be enough data, especially some data such as pore aspect ratio; we suggest that first the required data be estimated based on the available data
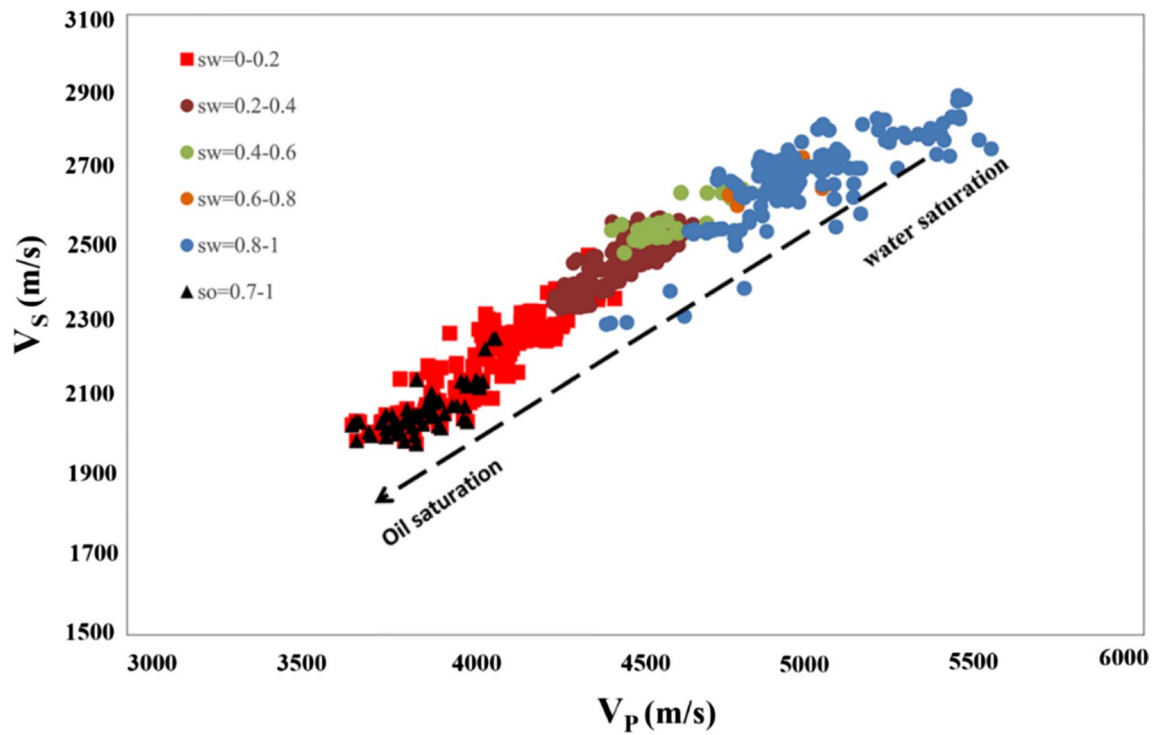
Fig. 14 The cross-plot of V_S against V_P is scaled by different oil and water saturation values
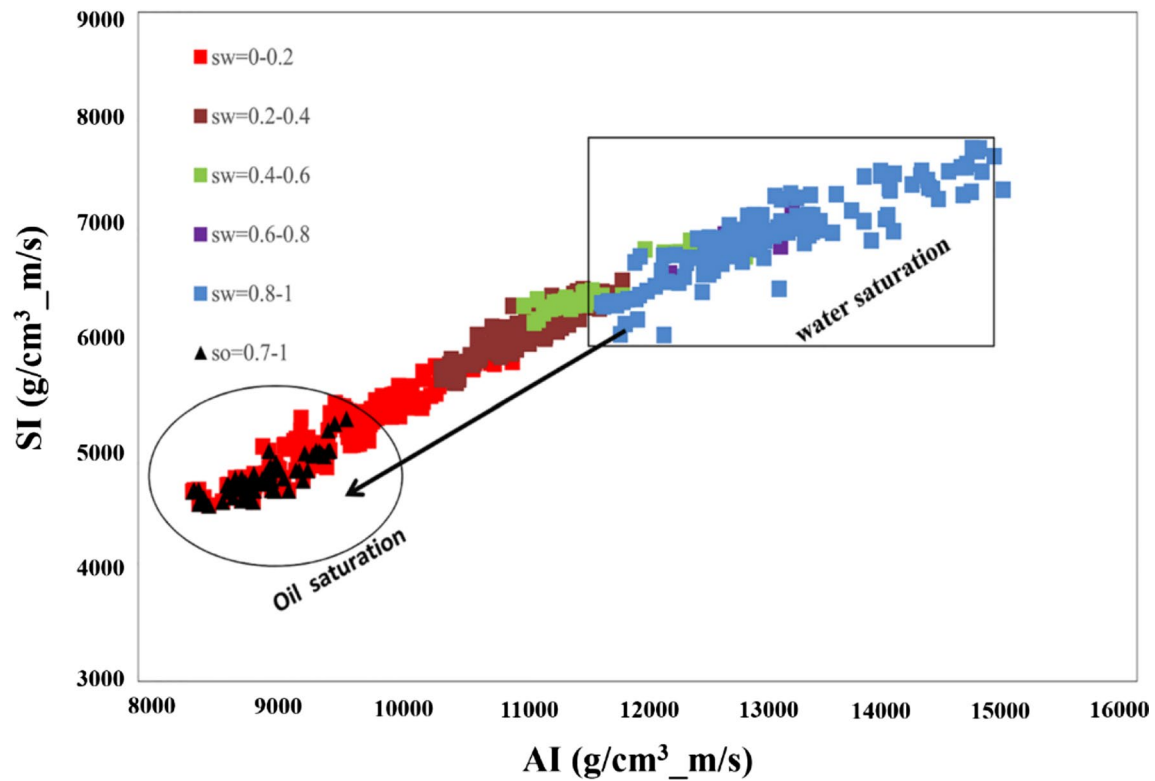

Fig. 15 The cross-plot of SI against AI was scaled by different oil and water saturation values

using artificial intelligence techniques, especially machine learning, and then the mathematical relationship between the parameters is discovered after the physical rock analysis.

Declarations

Conflict of interest On behalf of all authors, the corresponding author states that there is no conflict of interest.

References

Abe SJ, Akinyemi OD, Olatunbosun MO (2022) Rock physics diagnostic for enhancing characterization of reservoir sands within offshore field, Niger Delta. J Emerg Trends Eng Appl Sci 13(2):60–68

AbdollahieFard I, Sherkati S, McClay K, Haq BU (2019) Tectono-sedimentary evolution of the Iranian Zagros in a global context and its impact on petroleum habitats. Dev Struct Geol Tecton 3:17–28. https://doi.org/10.1016/B978-0-12-815048-1.00002-0

Afghah M (2016) Biostratigraphy, facies analysis of upper cretaceous-lower paleocene strata in South Zagros Basin (Southwestern Iran). J Afr Earth Sc 119:171–184. https://doi.org/10.1016/j.jafrearsci.2016.04.002

Ahmad QA, Ehsan MI, Khan N, Majeed A, Zeeshan A, Ahmad R, Noori FM (2022) Numerical simulation and modeling of a poroelastic media for detection and discrimination of geo-fluids using finite difference method. Alex Eng J 61(5):3447–3462. https://doi.org/10.1016/j.aej.2021.08.064

Alavi M (2004) Regional stratigraphy of the Zagros fold-thrust belt of Iran and its proforeland evolution. Am J Sci 304(1):1–20. https://doi.org/10.2475/ajs.304.1.1

Albakr MA, Abd N, Hasan S, Al-Sharaa GH (2022) Reservoir characterization and density velocity analysis by using rock physics and integrated multi-types post-stack inversion to identify hydrocarbon possibility and litho-prediction of Mishrif formation in kumaite and Dhafriyah oil fields, Southern Iraq. Geophys Prospect. https://doi.org/10.1111/1365-2478.13266

Asquith GB, Krygowski D, Henderson S, Hurley N (2004) Basic well log analysis. AAPG methods in exploration series, vol 16. https://doi.org/10.1306/Mth16823

Assefa S, McCann C, Sothcott J (2003) Velocities of compressional and shear waves in limestones. Geophys Prospect 51:1–13. https://doi.org/10.1046/j.1365-2478.2003.00349.x

Avseth P, Mukerji T (2002) Seismic lithofacies classification from well logs using statistical rock physics. Petrophysics 43(21):70–81

Avseth P, Mukerji T, Mavko G (2010) Quantitative seismic interpretation: applying rock physics tools to reduce interpretation risk. Cambridge University Press

Borgomano JV, Pimienta LX, Fortin J, Guéguen Y (2019) Seismic dispersion and attenuation in fluid-saturated carbonate rocks: effect of microstructure and pressure. J Geophys Res: Solid Earth 124:12498–12522. https://doi.org/10.1029/2019JB018434

Boxberg MS, Prévost JH, Tromp J (2015) Wave propagation in porous media saturated with two fluids. Transp Porous Media 107:49–63. https://doi.org/10.1007/s11242-014-0424-2

Cao Q, Ye X, Liu Y, Wang P, Jiang K (2022) Effect of different lithological assemblages on shale reservoir properties in the Permian Longtan Formation, southeastern Sichuan Basin: Case study of

Well X1. PLoS ONE 17(8):e0271024. https://doi.org/10.1371/journal.pone.0271024

Crain ER (2013) Welcome to Crain's Petrophysical Handbook. Online Shareware Petrophysics Training and Reference Manual. http://www.spec2000.net

Chenin J, Bedle H (2022) Unsupervised machine learning, multi-attribute analysis for identifying low saturation gas reservoirs within the deepwater Gulf of Mexico, and Offshore Australia. Geosciences 12(3):132. https://doi.org/10.3390/geosciences12030132

Cross NE, Singh SK, Al-Enezi A, Behbehani S (2022) Mixed carbonate-clastic reservoir characterization of the mid-Cretaceous Mauddud Formation (Albian), north Kuwait—implications for field development. AAPG Bull 106(2):289–319. https://doi.org/10.1306/08182119209

Das B, Chatterjee R (2018) Well log data analysis for lithology and fluid identification in Krishna-Godavari Basin, India. Arab J Geosci 11(10):1–12. https://doi.org/10.1007/s12517-018-3587-2

Deng C, Pan H, Fang S, Konaté AA, Qin R (2017) Support vector machine as an alternative method for lithology classification of crystalline rocks. J Geophys Eng 14(2):341–349. https://doi.org/10.1088/1742-2140/aa5b5b

Di L, Ping Y, Zhonghong W, Weiguang L, Ping C, Wei X (2021) Relative rock physics-driven seismic facies discrimination. In: SEG/AAPG/SEPM 1st international meeting for applied geoscience & energy. https://doi.org/10.1190/segam2021-3593763.1

Dong S, Wang Z, Zeng L (2016) Lithology identification using kernel fisher discriminant analysis with well logs. J Pet Sci Eng 143:95–102. https://doi.org/10.1016/j.petrol.2016.02.017

Elyasi A, Goshtasbi K, Hashemolhosseini H (2016) A coupled thermo-hydro-mechanical simulation of reservoir CO2 enhanced oil recovery. Energy Environ 27(5):524–541. https://doi.org/10.1177/0958305X16665545

Fawad M, Rahman MJ, Mondol NH (2021) Seismic reservoir characterization of potential CO2 storage reservoir sandstones in Smeaheia area, Northern North Sea. J Pet Sci Eng 205:108812. https://doi.org/10.1016/j.petrol.2021.108812

Fawad M, Hansen JA, Mondol NH (2020) Seismic-Fluid Detection-A Review. Earth Sci Rev 2020:103347. https://doi.org/10.1016/j.earscirev.2020.103347

Foster D, Zhao Z, Kumar D, Dralus D, Sen M (2021) Frequency-dependent AVO attributes for fluid saturation and thin-bed mapping. In: SEG/AAPG/SEPM 1st international meeting for applied geoscience & energy. https://doi.org/10.1190/segam2021-3582997.1

Gardner GHF, Gardner LW, Gregory AR (1974) Formation velocity and density—the diagnostic basics for stratigraphic traps. Geophysics 39:770–780. https://doi.org/10.1190/1.1440465

Gassmann F (1951) Elastic waves through a packing of spheres. Geophysics 16(4):673–685. https://doi.org/10.1190/1.1437718

Gelinsky S (2020) Reservoir characterization supported by rock physics diagnostics. In: Offshore technology conference Asia, Kuala Lumpur, Malaysia, November 2–August 19, 2020, Offshore Technology Conference, 2020, OTC-30359-MS. https://doi.org/10.4043/30359-MS

Grana D, Parsekian AD, Flinchum BA, Callahan RP, Smeltz NY, Li A, et al. (2022). Geostatistical rock physics inversion for predicting the spatial distribution of porosity and saturation in the critical zone. Math Geosc. https://doi.org/10.1007/s11004-022-10006-0

Greenberg ML, Castagna JP (1992) Shear-wave velocity estimation in porous rocks: theoretical formulation, preliminary verification and applications. Geophys Prospect 40:195–209. https://doi.org/10.1111/j.1365-2478.1992.tb00371.x

Hossain S, Junayed TR, Haque AKM (2022) Rock physics diagnostics and modelling of the Mangahewa Formation of the Maui B gas field, Taranaki Basin, offshore New Zealand. Arab J Geosci 15(13):1–21. https://doi.org/10.1007/s12517-022-10436-4

Huang C, Zhang X, Liu S, Li N, Kang J, Xiong G (2021) Construction of pore structure and lithology of digital rock physics based on laboratory experiments. J Pet Explor Prod Technol 11(5):2113–2125. https://doi.org/10.1007/s13202-021-01149-7

Ibrahim AF, Elkatatny S, Abdelraouf Y, Al Ramadan M (2022) Application of various machine learning techniques in predicting water saturation in tight gas sandstone formation. J Energy Resour Technol 144(8):083009. https://doi.org/10.1115/1.4053248

Islam MA, Yunsi M, Qadri SM, Shalaby MR, Haque AKM (2021) Three-dimensional structural and petrophysical modeling for reservoir characterization of the Mangahewa formation, Pohokura Gas-Condensate Field, Taranaki Basin, New Zealand. Nat Resour Res 30(1):371–394. https://doi.org/10.1007/s11053-020-09744-x

Karimian Torghabeh, A., Qajar, J., & Dehghan Abnavi, A. (2022). Characterization of a heterogeneous carbonate reservoir by integrating electrofacies and hydraulic flow units: a case study of Kangan gas field, Zagros basin. J Pet Explor Prod Technol. https://doi.org/10.1007/s13202-022-01572-4

Kordi M (2019) Sedimentary basin analysis of the neo-tethys and its hydrocarbon systems in the Southern Zagros Fold-Thrust Belt and Foreland Basin. Earth Sci Rev 191:1–11. https://doi.org/10.1016/j.earscirev.2019.02.005

Kuster GT, Toksöz MN (1974) Velocity and attenuation of seismic waves in two-phase media: part I. Theoretical Formulations Geophysics 39:587–606. https://doi.org/10.1190/1.1440450

Lan T, Zong Z, Yanwen F (2022) An improved seismic fluid identification method incorporating squirt flow and frequency-dependent fluid-solid inversion. Interpretation 11(1):1–66. https://doi.org/10.1190/int-2022-0053.1

Li H, Zhang J, Gao Q, Li X, Yang Z (2022) Quantitative prediction of porosity and gas saturation based on a new dual-porosity rock-physics model and Shuey's Poisson ratio for tight sandstone reservoirs. J Pet Sci Eng 216:110826. https://doi.org/10.1016/j.petrol.2022.110826

Li H, Zhang J (2018) Well log and seismic data analysis for complex pore-structure carbonate reservoir using 3D rock physics templates. J Appl Geophys 151:175–183. https://doi.org/10.1016/j.jappgeo.2018.02.017

Li S, Peng Z (2017) Seismic acoustic impedance inversion with multi-parameter regularization. J Geophys Eng 14:520–532. https://doi.org/10.1088/1742-2140/aa5e67

Mavko G, Mukerji T, Dvorkin J (2020) The rock physics handbook, 3. Cambridge University Press, UK

Mehrabi H, Bagherpour B, Honarmand J (2020) Reservoir quality and micrite textures of microporous intervals in the upper cretaceous successions in the Zagros Area, SW Iran. J Pet Sci Eng 192:107292. https://doi.org/10.1016/j.petrol.2020.107292

Mirhashemi M, Khojasteh ER, Manaman NS, Makarian E (2022) Efficient sonic log estimations by geostatistics, empirical petrophysical relations, and their combination: two case studies from Iranian hydrocarbon reservoirs. J Pet Sci Eng 213:110384. https://doi.org/10.1016/j.petrol.2022.110384

Mondal I, Singh KH (2022) Core-log integration and application of machine learning technique for better reservoir characterisation of Eocene carbonates. Indian Offshore Energy Geosci 3(1):49–62. https://doi.org/10.1016/j.engeos.2021.10.006

Nazeer A, Abbasi SA, Solangi SH (2016) Sedimentary facies interpretation of Gamma Ray (GR) log as basic well logs in Central and Lower Indus Basin of Pakistan. Geodesy Geodyn 7:432–443. https://doi.org/10.1016/j.geog.2016.06.006

Pang M, Ba J, Carcione JM, Picotti S, Zhou J, Jiang R (2019) Estimation of porosity and fluid saturation in carbonates from rock-physics templates based on seismic Q. Geophysics 84(6):1–12. https://doi.org/10.1190/geo2019-0031.1

Ødegaard E, Avseth PA (2004) Well log and seismic data analysis using rock physics templates. First Break 22(10):37–43. https://doi.org/10.3997/1365-2397.2004017

Qing F, Yan J, Wang J, Hu Q, Wang M, Geng B, Chao J (2020) Pore Structure and fluid saturation of near-oil source low-permeability turbidite sandstone of the Dongying Sag in the Bohai Bay Basin, East China. J Pet Sci Eng 196:108106. https://doi.org/10.1016/j.petrol.2020.108106

Radwan AA, Nabawy BS, Shihata M, Leila M (2022) Seismic interpretation, reservoir characterization, gas origin and entrapment of the Miocene-Pliocene Mangaa C sandstone, Karewa Gas Field, North Taranaki Basin, New Zealand. Mar Pet Geol 135:105420. https://doi.org/10.1016/j.marpetgeo.2021.105420

Singh A, Ojha M (2022) Machine learning in the classification of lithology using downhole NMR data of the NGHP-02 expedition in the Krishna-Godavari offshore Basin, India. Mar Pet Geol 135:105443. https://doi.org/10.1016/j.marpetgeo.2021.105443

Taheri A, Makarian E, Manaman NS, Ju H, Kim TH, Geem ZW, RahimiZadeh K (2022) A fully-self-adaptive harmony search GMDH-type neural network algorithm to estimate shear-wave velocity in porous media. Appl Sci 12(13):6339. https://doi.org/10.3390/app12136339

Teillet T, Fournier F, Zhao L, Borgomano J, Hong F (2021) Geophysical pore type inversion in carbonate reservoir: Integration of cores, well logs, and seismic data (Yadana field, offshore Myanmar). Geophysics 86(3):B149–B164. https://doi.org/10.1190/geo2020-0486.1

Temizel C, Odi U, Balaji K, Aydin H, Santos JE (2022) Classifying facies in 3D digital rock images using supervised and unsupervised approaches. Energies 15(20):7660. https://doi.org/10.3390/en15207660

Wang G, Lai J, Liu B, Fan Z, Liu S, Shi Y, Zhang H, Chen J (2020) Fluid property discrimination in dolostone reservoirs using well logs. Acta Geol Sin-Engl Ed 94:831–846. https://doi.org/10.1111/1755-6724.14526

Wang X, Zuo R, Wang Z (2022a) Lithological mapping using a convolutional neural network based on stream sediment geochemical survey data. Nat Resour Res 31(5):2397–2412. https://doi.org/10.1007/s11053-022-10096-x

Wang YR, Zong ZY, Yin XY (2022b) Fluid discrimination incorporating amplitude variation with angle inversion and squirt flow of the fluid. Pet Sci. https://doi.org/10.1016/j.petsci.2022.03.007

Wei D, Gao Z, Fan T, Zhang C, Tsau JS (2020) The rock-fabric/petrophysical characteristics and classification of the micropores hosted between the calcite and dolomite crystals. J Pet Sci Eng 193:107383. https://doi.org/10.1016/j.petrol.2020.107383

Wood AB (1955) A textbook of sound: being an account of the physics of vibrations with special reference to recent theoretical and technical developments. 3rd rev edn. Macmillan, New York

Xie JY, Zhang JJ, Xiang W, Fang YP, Xue YJ, Cao JX, Tian RF (2022) Effect of microscopic pore structures on ultrasonic velocity in tight sandstone with different fluid saturation. Pet Sci. https://doi.org/10.1016/j.petsci.2022.06.009

Xu C, Ding P, Di B, Wei J (2021) Investigation of fluid effects on seismic responses through a physical modeling experiment. Interpretation 9(1):T213–T222. https://doi.org/10.1190/INT-2020-0116.1

Xu S, Payne MA (2009) Modeling elastic properties in carbonate rocks. Lead Edge 28:66–74. https://doi.org/10.1190/1.3064148

Xu Z, Ma W, Lin P, Hua Y (2022) Deep learning of rock microscopic images for intelligent lithology identification: neural network comparison and selection. J Rock Mech Geotech Eng 14(4):1140–1152. https://doi.org/10.1016/j.jrmge.2022.05.009

Yang Q, Malcolm A (2021) Frequency domain full-waveform inversion in a fluid-saturated poroelastic medium. Geophys J Int 225(1):68–84. https://doi.org/10.1093/gji/ggaa579

Yang S, Wei J (2017) Fundamentals of Petrophysics, Springer Geophysics, vol 2. Springer, Berlin, Heidelberg

Zhou T, Rose D, Millot P, Grover R, Beekman S, Amin MFM, Zamzuri MDB, Ralphie B, Zakwan ZA (2018) Comprehensive neutron porosity from a pulsed neutron logging tool. In: SPWLA 59th annual logging symposium, London, UK, June 2018, Society of Petrophysicists and Well-Log Analysts, SPWLA-2018-XXX

Zhou, X., Ba, J., Santos, J. E., Carcione, J. M., Fu, L. Y., & Pang, M. (2021). Fluid discrimination in ultra-deep reservoirs based on a double double-porosity theory. Frontiers in Earth Science, 9, 649984. https://doi.org/10.3389/feart.2021.649984